Ionics (2009) 15:609–614
DOI 10.1007/s11581-008-0310-4

ORIGINAL PAPER

Studies on the effect of titanium addition on $LiCoO_2$

M. Ganesan

Received: 24 April 2008 / Revised: 18 November 2008 / Accepted: 10 December 2008 / Published online: 12 February 2009

Abstract The lithiated transition metal oxide has been used as the cathode materials for lithium ion rechargeable batteries. Among the various cathode materials, $LiCoO_2$ has been widely used. There are lot of reports on the substituted $LiCoO_2$ replacing small amount of Cobalt with other transition and nontransitional metals. Here, we focus on to a tetravalent transition metal atom such as titanium, as an addition in $LiCoO_2$ and studied its performance. The titled cathode material was synthesized by solid-state reaction method. Thermogravimetric/differential thermal analysis, X-ray diffraction, X-ray fluorescence, scanning electron microscopy, and particle size analysis were carried out to assess the effect of addition of titanium on $LiCoO_2$. Electrochemical studies were carried out by cyclic voltammetry and life cycle analyzer.

Keywords Ceramics · Oxides · Electrochemical techniques · Electrochemical properties · Chemical synthesis

Introduction

Lithium rechargeable batteries offer the highest energy density of all rechargeable battery systems [1] and offer various applications. The requirements for advanced lithium rechargeable batteries include high energy and power density, reversibility, cyclability, safety, and low cost [1, 2]. Recent developments on lithium batteries have shown that some of the AMO_2 layered oxides such as $LiNiO_2$ and $LiCoO_2$ as materials of interest for positive electrodes of rechargeable lithium ion batteries. Moly Energy utilizes $LiNiO_2$ [3] and Sony Energytec $LiCoO_2$ [4] were used in lithium and lithium ion batteries. These types of batteries are being developed for a variety of applications ranging from solid-state microbatteries and electric vehicle applications.

$LiCoO_2$ and $LiNiO_2$ adopt a layer structure with prototyped α-$NaFeO_2$ and space group of R3m with a hexagonal setting comprising basically the lithium ions in the 3b sites, the transition metal ions in the 3a sites, and the oxide ion in the 6c sites. During charging and discharging process, removal of lithium ions in $LiCoO_2$ and $LiNiO_2$ tends to destabilize the crystal structure due to increasing repulsion between the bare oxide layers that face each other. The advantage of $LiCoO_2$ over $LiNiO_2$ is that a significant higher number of lithium ions can be removed upon charging before the structure becomes unstable with respect to displacement of the transition metal oxide. To compare the preparation of $LiNiO_2$, $LiCoO_2$ electrode system is relatively easy and safe. In addition to this, $LiCoO_2$ material shows good reversibility and cyclability due to its Co^{3+}/Co^{4+} redox reaction. The main aim for the most of the researchers is to develop and optimize different cathode materials for replacing the high cost and toxic nature of $LiCoO_2$ cathode material, which is still the main cathode material for the most of commercial lithium ion batteries. However, $LiCoO_2$ shows relatively great capacity fading after extended cycling, i.e., when lithium ion becomes deintercalated above 4.2 V. This was reported due to anisotropic expansion and contraction during cycling [5–10]. Our present study is to improve the electrochemical behavior of $LiCoO_2$ by means of addition of tetravalent transition metal ion Ti^{4+} in $LiCoO_2$. This titanium-substituted transition metal oxide is both lighter

M. Ganesan (✉)
Central Electro Chemical Research Institute,
Karaikudi 630006, India
e-mail: mgshan2002@yahoo.co.in

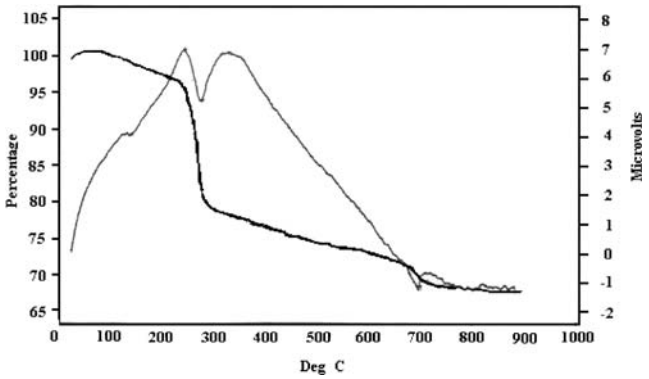

Fig. 1 TG/DTA curve for $LiCoTi_{0.5}O_2$

and less expensive and exhibits higher voltage than bare oxide. $LiNi_{0.8y}Ti_yCo_{0.2}O_2$ [11], $LiNi_{0.8}Co_{0.1}Ti_{0.1}O_2$ [12], and $LiCo_{1-x}Ti_xO_2$ [13] were reported already with improved cycling performance and enhanced thermal stability. Here, an attempt has been made to add a half mole of tetravalent titanium on $LiCoO_2$. The addition of titanium is done through solid-state reaction method. The effect of titanium-added material on the structural and electrochemical properties were studied through X-ray diffraction (X-RD), X-ray fluorescence (X-RF), scanning electron microscopy (SEM), and particle size analyzer. Electrochemical studies have been carried out to determine the capacity, reversibility, and cyclability.

Experimental

The titled cathode material was prepared by reacting stoichiometric amount of lithium carbonate and cobalt carbonate required for synthesizing $LiCoO_2$ along with a half mole of titanium dioxide. The above materials were grained well to get homogeneous mixture which was heated in the furnace at 900 °C for 72 h in air. In this solid-state reaction method continuous heating and grinding plays a major role to make the compound homogenous and to get reduced particle size. Thermal decomposition behavior of the dried precursor was examined in air using STA 1500 thermogravimetric/differential thermal analyzer (TG/DTA) from room temperature to 900 °C at 20 °C/min. X-ray diffraction analysis has been taken to confirm the formation of compound by using X-ray diffractometer (JEOL-JDX 8030 X-ray diffractometer, λ=1.5406 Å using nickel filtered Cu kα). Surface morphology studies were carried out through Hitachi S-3000 H scanning electron microscopy. X-RF measurements were done by Horiba XGT 2700 X-ray analytical microscope. Particle size distribution was carried out using Horiba LA-910 laser scattering particle size analyzer. A computer-controlled Bitrode (USA) Life cycle tester was used for cycle tests.

Cell preparation

A mixer of synthesized cathode material with 10% acetylene black and 5% polyvinylidene fluoride in *N*-methylpyrrolidone slurry was used to prepare the electrodes. This slurry was then brush-coated on an aluminum foil substrate, which is previously pickled in NaOH, washed with distilled water, degreased with acetone, and dried in a vacuum oven maintained at 110 °C for 12 h. The 2016 coin type cells were assembled in glove box filled with inert gas (argon) by sandwiching the prepared cathode material with lithium metal as anode separated by a polypropylene separator soaked in the ethylenecarbonate (EC) and dimethylcarbonate (DMC; 1:1) mixture with $LiPF_6$ electrolyte. The cells were crimp sealed. Electrochemical studies were carried out using an Autolab PGSTAT 30, controlled by GPES-4.9 software. Lithium foil was used as both reference and auxiliary electrodes for electrochemical studies; hence, potentials are referred to the Li/Li^+ reference electrode [14].

Results and discussion

Figure 1 display the TG and DTA for $LiCoTi_{0.5}O_2$ solid precursor. TG records the weight loss of the sample with respect to temperature from 20 °C to 900 °C. The TG/DTA behavior for synthesized cathode materials by solid-state reaction method shows four distinct regions. $LiCoO_2$ and $LiCoTi_{0.5}O_2$ behave similarly. The region up to 233.6 °C with a weight loss of 4% may be accounted for the moisture entrapped in the precursor sample. While in the second region (233–297 °C) may be attributed to reaction of Li_2CO_3 and $CoCO_3$ enter into in air [15]. $CoCO_3$ undergoes an endothermic reaction to yield Co_3O_4 around 276 °C, which is displayed in the DTA curve for $LiCoO_2$ [15, 16]. The observed exothermic peak is mainly due to a possible reaction between the finely divided Co_3O_4 and Li_2CO_3 to form Co_3O_4 with interfacial Li_2O [15]. The results are not surprising given the fact that several carbonates upon

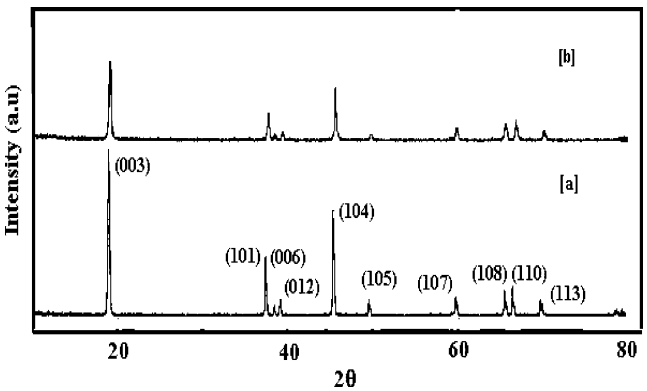

Fig. 2 X-ray diffraction of *a* $LiCoO_2$ and *b* $LiCoTi_{0.5}O_2$

Table 1 Lattice parameters calculated by least square method for $LiCoO_2$ and $LiCoTi_{0.5}O_2$

	a	*c*	*c*/*a*	I_{003}/I_{104}
$LiCoO_2$	2.81	14.01	5.018	2.26
$LiCoTi_{0.50}O_2$	2.806	14.153	5.044	1.76

mixing produce easily decomposable mixtures [17]. Finally, the $LiCoO_2$ is formed at 712.63 °C. This further heating up to 900 °C shows no weight loss is observed in TG/DTA profile, which indicates completion of reaction and the compound is formed.

Figure 2 illustrated the X-ray diffractograms for the synthesized $LiCoO_2$ and $LiCoTi_{0.5}O_2$ calcined at 900 °C up to 72 h. By the presence of sharp diffractograms of higher intensity peak, the phase pure compound with better crystallinity is achieved. All the peaks are indexable to hexagonal α-$NaFeO_2$ layered structure with (R3m) group as a result of the strong peak located at approximately 2θ=19° and with the medium intensity peaks located at 2θ=36° and 44°. It is observed from the X-ray patterns that the entire

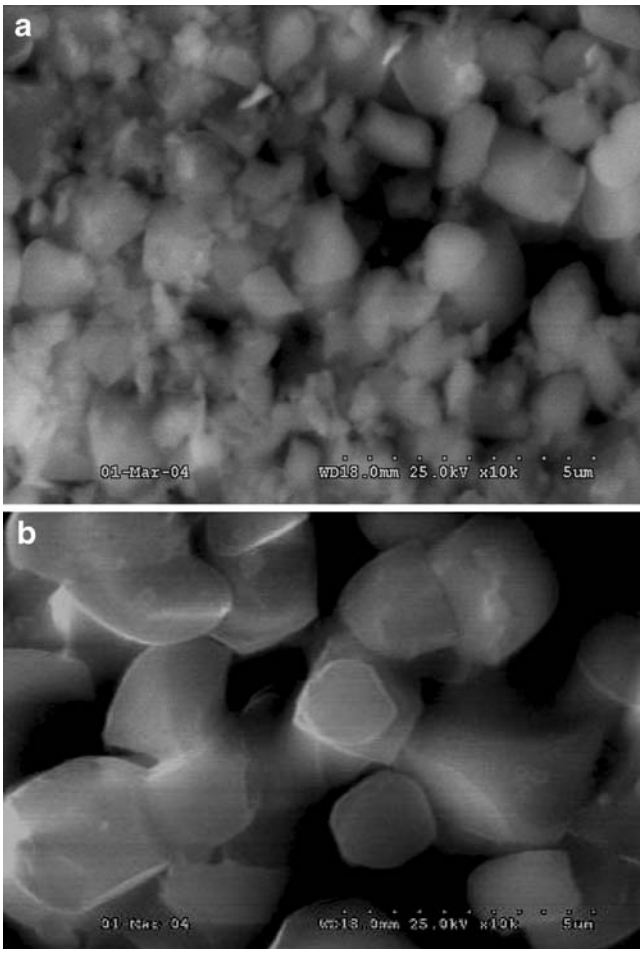

Fig. 3 **a** SEM micrograph of $LiCoO_2$ (magnification ×10K); **b** SEM micrograph of $LiCoTi_{0.5}O_2$ (magnification ×10K)

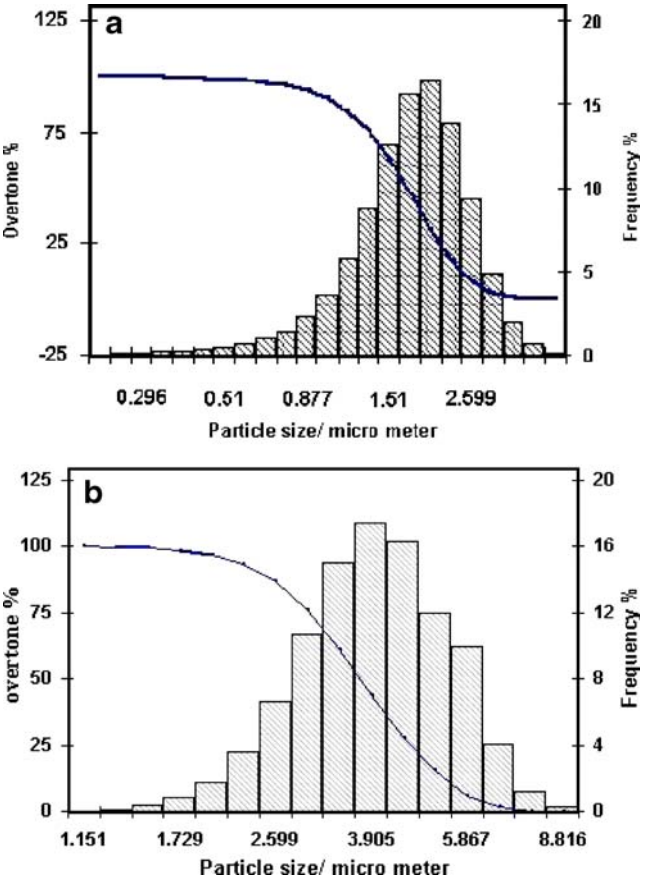

Fig. 4 **a** Particle size distribution of $LiCoO_2$; **b** particle size distribution of $LiCoTi_{0.5}O_2$

fingerprint peaks, viz., (003, 101, 006, 012, 104, 105, 107, 108, 110, and 113) are clearly identifiable thereby suggesting the formation of the α-$NaFeO_2$ structure. These diffracted peaks are in excellent agreement with the (JCPDS card No. 16-0427). $LiCoO_2$ is less sensitive to synthesis condition due to their higher degree of covalent bond in the CoO_2 slabs, and single-phase pure compound is normally obtained through solid-state reaction of Li salts

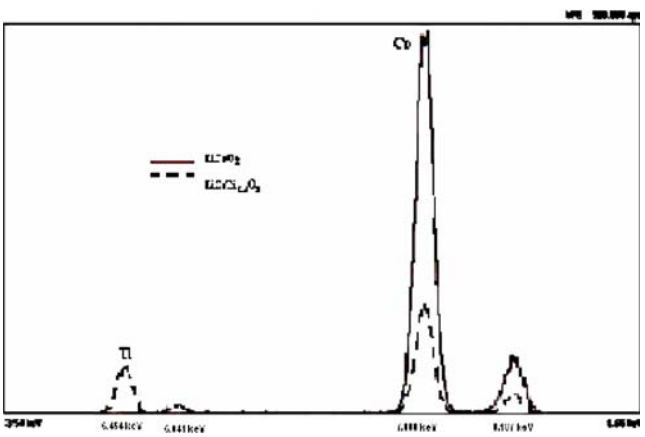

Fig. 5 X-RF diagram of $LiCoO_2$ and $LiCoTi_{0.5}O_2$

and Co oxides. The diffracted peaks at (003)/(104) with high intensity with clear splitting of (006)/(012) and (108)/(110) signifying that this samples were well developed layered $LiCoO_2$ structure [18]. When the inclusion of half mole of titanium, the peak becomes slightly broaden and the intensity of peak is decreased, which indicates the crystallization is weakened for the titanium-doped materials [11]. The two characters of X-RD patterns, i.e., I_{003}/I_{004} ratio and 108/110 or 006/012 peak splitting, were the main criteria for the degree of ordering in layered structure as well as the amount of transition metal in the inter slab space [19, 20]. The structure of $LiCoTi_{0.50}O_2$ is basically identical, and this indicates that the introduction of titanium into a $LiCoO_2$ does not affect the local structure of Co. Furthermore, the lattice constant *a* and *c* were calculated via least-square refinement method using ten well-defined diffraction lines with indexation in the hexagonal system. These values are given in Table 1.

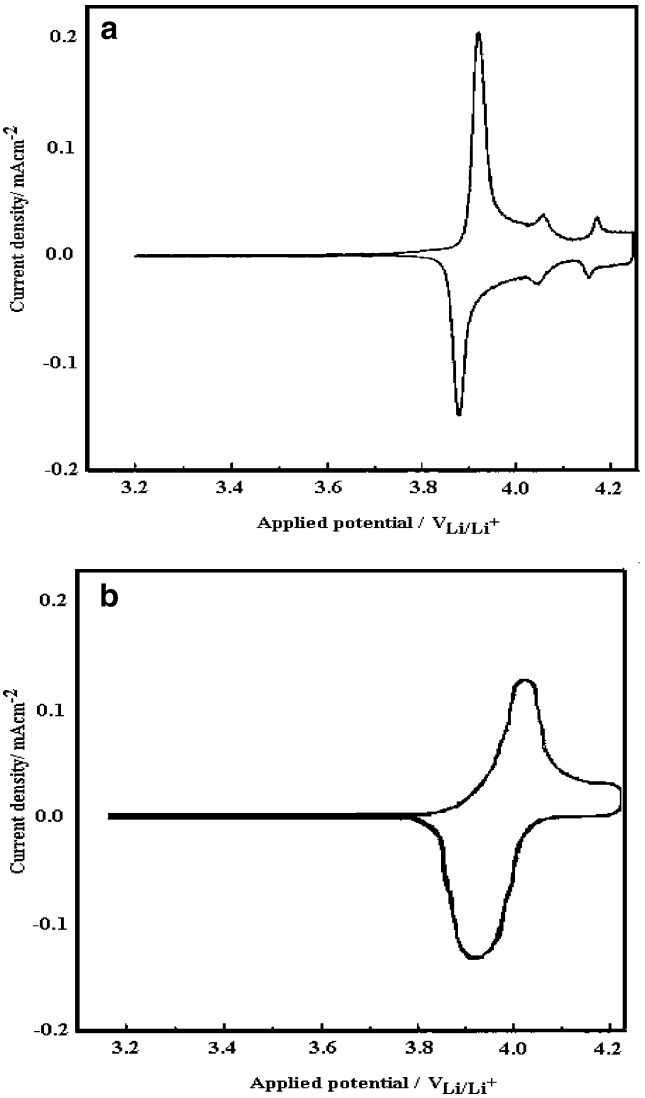

Fig. 6 **a** Cyclic voltammogram of $LiCoO_2$ (scan rate, 1 mV/s); **b** cyclic voltammogram of $LiCoTi_{0.5}O_2$ (scan rate, 1 mV/s)

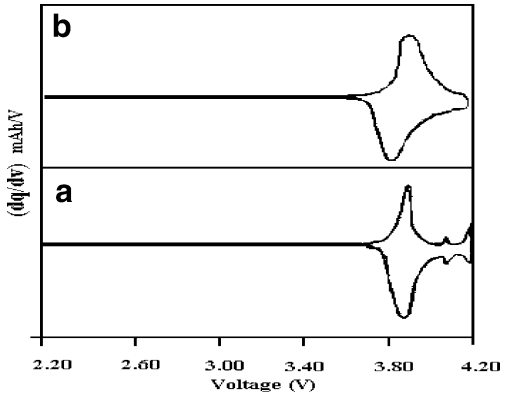

Fig. 7 The derivative graph drawn from second charge–discharge data of **a** $LiCoO_2$ and **b** $LiCoTi_{0.5}O_2$

The SEM photograph for $LiCoO_2$ and $LiCoTi_{0.50}O_2$ were shown in Fig. 3a, b. These two figures have similar morphologies. They exhibited a random distribution of smaller and bigger particle. The particle morphology plays a critical role in battery performance, especially for high-power applications. This morphology improves material safety characteristics because the particles have relatively smaller surface areas, which reduces the reactivity between

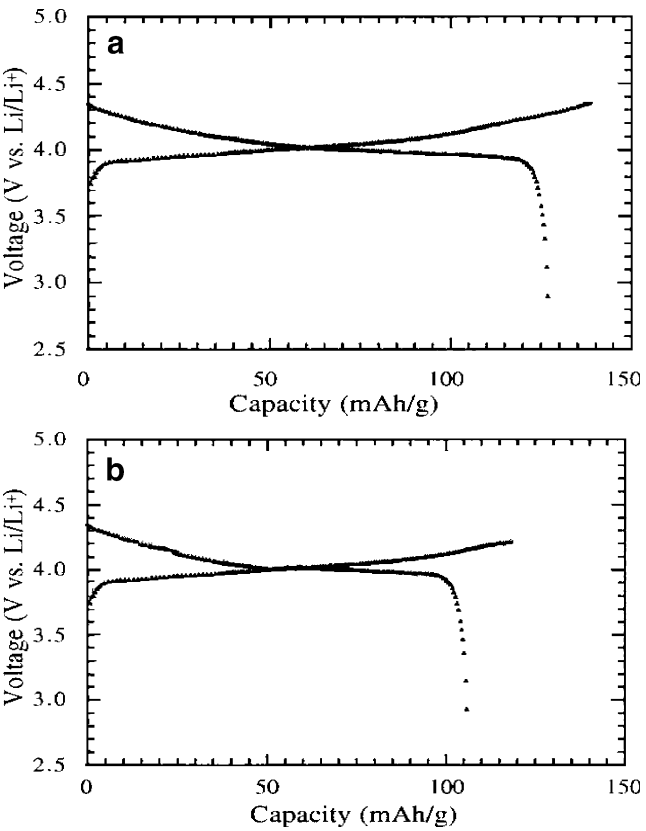

Fig. 8 **a** Initial charge–discharge characteristic curve of $LiCoTi_{0.5}O_2$; **b** charge–discharge curve after tenth cycle of $LiCoTi_{0.5}O_2$

the solid electrode materials and the liquid electrolyte. Furthermore, the size of the particle is analyzed by using the particle size analyzer, which is depicted in Fig. 4a, b. The results shows that the average size of the particle obtained by this solid-state reaction method is 1.46 μm for $LiCoO_2$ and 4.484 μm for $LiCoTi_{0.50}O_2$, which is suitable for high-power applications. The effect of particles size on the electrochemical behavior of the cathodes can also be considered, as it is stated that the cyclic stability of $LiCoO_2$ with 2–4-μm-size particles was found to be better than the one with 5–10-μm-size particles.

The X-ray fluorescence spectroscopy for the synthesized cathode materials is shown in Fig. 5. With the use of this peak, we can able to account for the composition of cobalt and titanium present in the prepared materials. The two peaks, which were observed for both titanium and cobalt, are the one with the high intensity peak that is due to primary X-rays and the other one that is due to secondary X-rays. By the presence of very high intensity peak for cobalt with the absence of any other peaks obviously indicates that the prepared $LiCoO_2$ is free from impurities. While in $LiCoTi_{0.50}O_2$, the peak intensity for cobalt is largely suppressed due to the half mole of tetravalent titanium introduced in the native compound. Furthermore, it is identified (Fig. 5) that the incorporation of titanium cannot affect the local environment of cobalt. X-RD analysis also supports the same. Thus, the stoichiometries of the synthesized compounds were assessed and it was in accordance with our aimed composition.

Electrochemical characterization

The cyclic voltammogram (CV) for $LiCoO_2$ was performed at the low scan rate, which enables the scanning of potential of working electrode in both anodic and cathodic direction, i.e., the potential can be reversed. Figure 6a illustrates CV of $LiCoO_2$, which was obtained with $LiCoO_2$ as the working electrode and lithium as both the counter and reference electrodes. At low sweep rates, most of the Li^+ has been removed from $LiCoO_2$ and the electrode equilibrium potential is more positive. Hence, on reversing the sweep, the current polarity immediately changes (positive to negative) corresponding to Li^+ intercalation. The same effect causes the shift of the peak currents during the reverse sweep. At low scan rates, the time for Li^+ insertion is large, and hence, the peak appears much earlier as

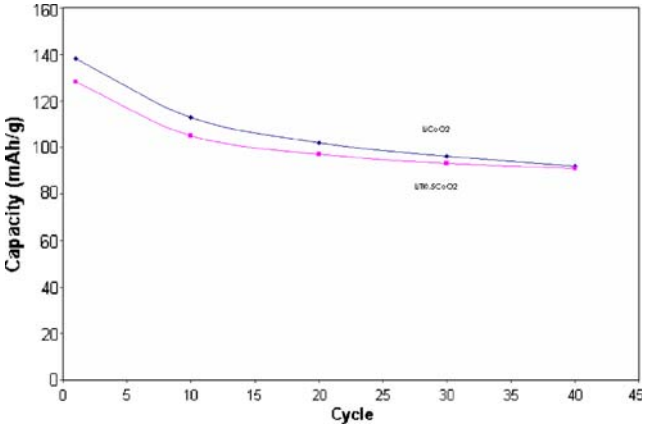

Fig. 9 Capacity dependences on cycle for $LiTi_{0.5}CoO_2$ and $LiCoO_2$

compared to high sweep rates. The forward scan is associated with charging the cell and the reverse with discharging the cell. From these figures, three sets of well-defined peaks appear during both the charging and discharging process. If lithium is used as the counter electrode, all the active material from $LiCoO_2$ is removed and peaks appear during the forward scan 3.92 V, while in the reverse sweep, the peak appears at 3.89 V, respectively, and these peaks are first-order phase transitions. This is mainly due to the lithium deintercalation/intercalation into the intercalation sites, which is due to two pseudo-phases of lithium dilute α-phase and lithium concentrated β-phase [21]. The second and third sets of peaks are observed at (4.055, 4.060) and (4.174, 4.164 V), respectively. This may be because of the order/disorder phase transition, respectively [7]. But in the case for $LiCoTi_{0.5}O_2$ (Fig. 6b), the peak shifted to the higher potential, and the higher voltage peaks are highly shrunk. These results are well reflected in the derivative curve obtained from the second charge–discharge cycle data as shown in Fig. 7. From the results, the high voltage peak observed here are attributed to continuous phase transitions and that the high voltage peaks are not due to anion adsorption on surface impurities [22]. The profile of the CV does not differ with cycling, while the magnitude of the peak changes drastically for $LiCoTi_{0.5}O_2$. This indicates inclusion of titanium that could suppress the phase transition and also change the surface of the $LiCoO_2$ electrode with cycling. This change in surface layer could have increased the positive electrode resistance; thereby, it decreases the charge and discharge currents.

Table 2 Charge–discharge capacity for $LiCoO_2$ and $LiCoTi_{0.5}O_2$

	Initial charge capacity ($mAhg^{-1}$)	Initial discharge capacity ($mAhg^{-1}$)	Loss of (%)	After10 cycles charge capacity ($mAhg^{-1}$)	After10 cycles discharge capacity ($mAhg^{-1}$)	Loss of (%)
$LiCoO_2$	150	138	8.6	132	113	16.8
$LiCoTi_{0.5}O_2$	140	128	9.3	123	105	17.1

The charge–discharge characteristics is performed with the electrolyte 1:1 EC/DMC along with 1 M $LiPF_6$ between 2.7 and 4.2 V vs Li/Li^+ electrodes for prepared cathode material, with the charge–discharge rate of C/5. $LiCoO_2$ delivers an initial charge capacity of 150 $mAhg^{-1}$ during charging and 138 $mAhg^{-1}$ during discharging process with the loss of 8.6%, while in the case of $LiTi_{0.5}CoO_2$, it gave 140 and 128 $mAhg^{-1}$ during charging and discharging process, respectively, with the loss of 9.3% as shown in Fig. 8a. This fading in capacity may be attributed mainly due to the poor lithium ion diffusivity, resulting from the presence of titanium in both tetrahedral and octahedral sites. This may be one of the reasons for capacity fading. However, the incorporation of half molecule of titanium in $LiCoO_2$ favors and maintains the layered structure by forming the solid solution with same structure (R3m), which is observed from the X-RD pattern of $LiCoTi_{0.5}O_2$. Furthermore, the charge–discharge test carried out after ten cycles for $LiTi_{0.5}CoO_2$ is presented in Fig. 8b. From this, the basic shape of the charge and discharge curves remains the same after cycling; the charge and discharge capacity decreases with increasing cycle number, which is given in Fig. 9. After ten cycles, the discharge capacity drops to 113 $mAhg^{-1}$ for $LiCoO_2$, while for $LiCoTi_{0.5}O_2$, it is 105 $mAhg^{-1}$ (Table 2). The initial capacity losses of the cathodes in this work do not increase with the increase of extra transition metal at the 3a sites as observed in [11]. This may be attributed to the improved structural stability during cycling and lower oxidation ability at high delithiated state. Decrease of the capacity losses originated from lattice change and interface reaction compensates the increase of the capacity losses caused by the extra transition metal at the 3a Li site. This decrease in specific capacity for titanium-added $LiCoO_2$ is comparable to those of $LiCoO_2$. Furthermore, the addition of titanium can enhance the cycle, as well as its stability [11].

Conclusion

$LiCoO_2$ and $LiCoTi_{0.5}O_2$ materials were synthesized through solid-state reaction method. The formation temperature was found to be 712.63 °C through TG/DTA analysis. X-RD studies, complemented by X-RF diagram, show that the synthesized materials are phase pure stoichiometric compound. Based on the electrochemical studies for the synthesized compounds, the following conclusions can be arrived at:

1. The high voltage peaks observed on CV are attributed to continuous phase transitions and not only due to anion adsorption on surface impurities, which indicates addition of titanium could suppress the phase transition, but also changes in the surface of the $LiCoO_2$ electrode with cycling. This change in surface layer could have increased the positive electrode resistance, thereby decreasing the charge and discharge currents.
2. This fading in capacity for $LiTi_{0.5}CoO_2$ may be attributed mainly due to the poor lithium ion diffusivity, resulting from the presence of titanium in both tetrahedral and octahedral sites. This may be one of the reasons for capacity fading.

Acknowledgments Author thanks Director, CECRI for his permission to publish this paper and thank MNES, India for their funding.

References

1. Scrosati B (1995) Nature 373:557
2. Brandt K (1994) Solid State Ion 69:173
3. Nagaura T, Tozawa K (1990) Prog Batteries Solar Cells 9:209
4. Dahn JR, von Sacken U, Juzkow MW, Al-Janaby H (1991) J Electrochem Soc 138:2207
5. Wang H, Jang Y-I, Huang B, Sadoway DR, Chiang Y-M (1999) J Electrochem Soc 146:473
6. Ohzuku T, Ueda A (1994) J Electrochem Soc 141:2972
7. Reimers JN, Dahn JR (1992) J Electrochem Soc 139:2091
8. Cho J, Kim YJ, Park B (2000) Chem Mater 12:3788
9. Cho J, Kim YJ, Park B (2001) J Electrochem Soc 148:A1110
10. Cho J, Kim YJ, Kim T-J, Park B (2001) Angew Chem Int Ed Engl 40:3367
11. Liu H, Li J, Zhang Z, Gong Z, Yang Y (2004) Electrochim Acta 49:1151
12. Arai H, Tsuda M, Sakurai Y (2000) J Power Sources 90:76
13. Gopukumar S, Jeong Y, Kim KB (2003) Solid State Ion 159:223–232
14. Wang GX, Zhong S, Brahurst DH, Dou SX, Liu HK (1998) J Power Sources 76:141
15. Lundbald A, Bergman B (1997) Solid State Ion 96:173
16. Ahmed AI, EI-Hakam SA, Samra SE (1990) Ind J Chem Sec A 29:470
17. Malik WU, Gupta DR, Masood I, Gupta RS (1985) J Mat Sci Lett 4:532
18. Gummow RJ, Thackeray MM, David WIF, Hull S (1992) Mater Res Bull 27:327
19. Li W, Reimers JN, Dahn JR (1993) Solid State Ion 67:123
20. Peres JP, Delmas C, Rougier A, Broussely M, Perton F, Biensan P, Willmann P (1996) J Phys Chem Solids 57:1057
21. Choi YM, Pyun SI, Bae JS, Moon SI (1995) J Power Sources 56:25
22. Yazami R, Lebrun N, Bonneau M, Molteni M (1995) J Power Sources 54:389